Optimising resistive charge-division strip detectors for low energy charged-particle spectroscopy

SMITH, Robin <http://orcid.org/0000-0002-9671-8599>, BISHOP, Jack, KOKALOVA, Tz., WHELDON, Carl, FREER, Martin, CURTIS, Neil, HAIDER, Zeshan and PARKER, D.J.

Published version

SMITH, Robin, BISHOP, Jack, KOKALOVA, Tz., WHELDON, Carl, FREER, Martin, CURTIS, Neil, HAIDER, Zeshan and PARKER, D.J. (2018). Optimising resistive charge-division strip detectors for low energy charged-particle spectroscopy. Nuclear Instruments and Methods in Physics Research Section A Accelerators Spectrometers Detectors and Associated Equipment, 901, 14-20.

Copyright and re-use policy

Accepted Manuscript

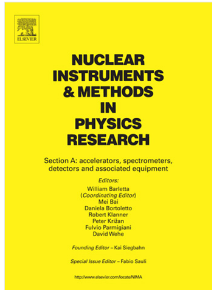

Optimizing resistive charge-division strip detectors for low energy charged-particle spectroscopy

R. Smith, J. Bishop, Tz. Kokalova, C. Wheldon, M. Freer, N. Curtis, Z. Haider, D.J. Parker

PII: S0168-9002(18)30671-5
DOI: https://doi.org/10.1016/j.nima.2018.05.052
Reference: NIMA 60836

To appear in: *Nuclear Inst. and Methods in Physics Research, A*

Received date : 26 April 2018
Accepted date : 24 May 2018

Optimizing resistive charge-division strip detectors for low energy charged-particle spectroscopy

R. Smith⋆[1], J. Bishop[1], Tz. Kokalova[1], C. Wheldon[1], M. Freer[1], N. Curtis[1], Z. Haider[1], D. J. Parker[1]

[1] *School of Physics and Astronomy, University of Birmingham, Edgbaston, B15 2TT*

Abstract

Two novel approaches to improving the signal-to-background ratio (SBR) for silicon resistive charge-division strip detectors (RSDs), when performing low energy charged-particle spectroscopy, are presented. Firstly, the normally-unutilized rear contact of the detector was used to veto events where the charge collected by this rear face did not match the sum of the charges collected by the strips on the front. Secondly, leading edge discriminator time walk was used to determine complementary information about the hit position along a strip. Using this alongside the position extracted from the charge division allowed clearer identification of true events over background, leading to an improved SBR. These methods were tested by measuring radiation from a triple-α source and then the ^{12}C(^{4}He,α)$\alpha\alpha\alpha$ breakup reaction at 40 MeV beam energy. The first method was found to improve the SBR by a factor of 4.0(2). The second method gave a SBR improvement of factor of 3.7(4). When both methods are applied together, a total improvement by a factor of 5.7(3) was measured.

Keywords: Charged-particle spectroscopy, semiconductor strip detectors
PACS: 29.40.Gx, 25.55.-e, 29.30.Ep

1. Introduction

Position-sensitive silicon strip detectors (PSDs) are essential for modern nuclear physics experiments involving the measurement of charged particles [1, 2]. In many cases, it is crucial to know both the position (direction) of incidence and the energy of a particle in order to determine the full kinematics of the reaction being measured. Such detectors typically come in two forms, double-sided silicon strip detectors (DSSDs) and resistive charge-division strip detectors (RSDs), which are shown schematically in Figs. 1 and 2, respectively.

Intrinsically, DSSDs and RSDs work in a similar way [3]. The front and rear faces consist of *p*-type and *n*-type semiconductor layers respectively, with a reverse bias applied across an electrode layer on each side. The resulting depletion region provides the detection medium and electron-hole pairs, excited by an incident charged particle, are collected by the electrodes on each detector face. The collected charge is proportional to the energy deposited by the particle.

⋆Current address: Sheffield Hallam University
Email address: Robin.Smith@shu.ac.uk (R. Smith⋆)

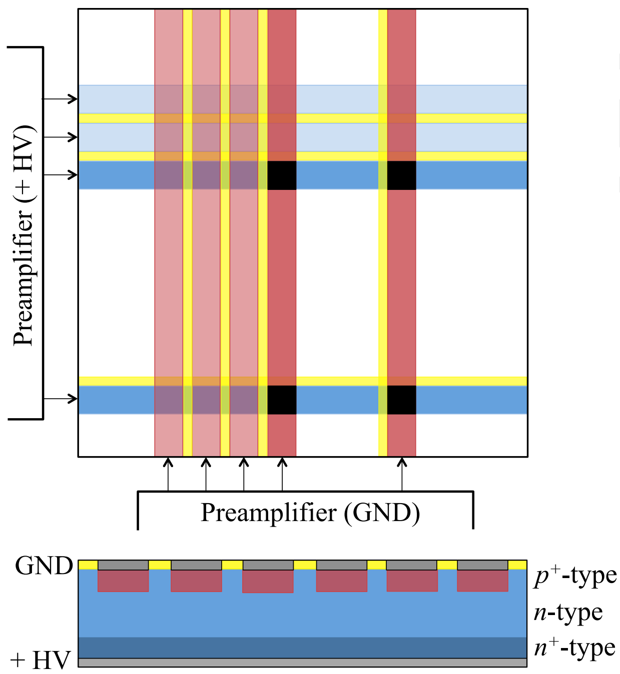

Figure 1: (color online) Schematic diagram of a double-sided silicon strip detector. The upper image shows the face of the detector and the lower image shows the cross section through the detector. When two particles hit the detector, four strips collect charge (two vertical on the front and two horizontal on the rear), which are highlighted in a darker shade. The crossing points in black mark the possible hit points. If the particles are sufficiently close in energy it is not possible to determine which two points are correct.

The DSSD electrodes are segmented into horizontal strips (rear) and vertical strips (front), which are built from low-resistance aluminium and isolated by a thin SiO_2 inter-strip region. Each strip has a separate readout. This means that by matching the charge collected on a single front strip with that of a single rear strip (within the detector resolution) the 2D position of a hit can be determined by their crossing point. The position resolution is therefore defined by the width of each strip. When multiple particles hit the detector simultaneously, the signals collected by the front and rear strips are seperately ordered in energy. Front and rear strips corresponding to the same particle will measure a similar energy. These detectors are ideal for high multiplicity events since they permit large solid angle coverage while minimising pile-up [4].

However, problems arise when the energies of the detected particles are very similar. In this case, energy-matching strips on the front and rear faces can produce a large number of possible crossing points (scaling with the square of the multiplicity). This can result in the incorrect assignments of the hit positions for the detected particles. For example, this crossing point ambiguity remains the largest source of background in determining the breakup branching ratio of the Hoyle state, which is of interest from a nuclear structure and astrophysical perspective [5, 6, 7]. Due to the proximity of the Hoyle state to the 3α decay threshold, the α particles emitted during the breakup have similar energies.

An RSD can provide a platform to more accurately measure the kinematics of these types of reactions, due to the way in which the position of a hit is determined. Like the DSSD, the front face of an RSD is split into a number of vertical strips, but each carry a ~kΩ resistance, and a signal is taken from each end. The rear face of the RSD is not segmented and is used in biasing the detector. Due to the strip resistance, the collected signal is linearly attenuated by an amount depending on the distance from the hit point to the ends of each strip. The position of a hit along a strip is calculated by combining the signals recorded at each end as [8]

$$f = A\left(\frac{Q_{\mathrm{H}} - Q_{\mathrm{L}}}{Q_{\mathrm{H}} + Q_{\mathrm{L}}}\right). \tag{1}$$

The signals collected at the *high* and *low* ends of a strip are labelled as Q_{H} and Q_{L}, f is the fractional position along the strip ($-1 \leq f \leq 1$) and A is a constant to account for the two 1 kΩ resistors in series with the strip (see Fig. 2). This method removes the ambiguity regarding multiple crossing points, which is a feature of DSSDs, and leads to clearer measurements of coincident particles with similar energies, if they strike separate strips. The charge division method has been shown to give superior position resolution compared to the DSSD strip width [9] but this is strongly dependent on the noise environment and the energies of the detected particles [10]. For high energy particles, a position resolution of 0.1 mm has previously been obtained. In this study, for low energy particles, a resolution of several mm was observed.

However, problems arise when an incident particle has a low energy or if it impacts the detector at the extreme ends of a strip. For example, consider the case where a particle strikes the strip shown in Fig. 2 at point 1. Due to the differences in resistance between the two paths taken, signal Q_H is largest and signal Q_L is highly attenuated. Depending on the energy of the initial hit, the signal Q_L may have a similar amplitude to the baseline electronic noise of the system. The same will occur when measuring a low energy particle anywhere along the strip. In order to record such events, the discriminator thresholds must be lowered towards the level of the noise, which inevitably leads to a higher chance of triggering on noise and recording background. In the past, these detectors were most commonly used for higher energy charged-particle spectroscopy, where typical thresholds of 3 MeV were applied. More modern strip detectors can operate with lower thresholds [11]. Nonetheless, these still significantly exceed the detection thresholds for DSSDs which are often set well below 1 MeV. Furthermore, since the active area of the detector is separated into just 16 channels, these detectors are more susceptible to pile-up. Despite these pitfalls, for the reasons previously discussed, the use of RSDs is advantageous under certain circumstances.

In this paper we present two methods of improving the performance of RSDs for charged particle spectroscopy. Both are implemented in the experimental hardware and require varying degrees of analysis in post-processing software. The first method utilises the energy signal from the rear contact of the detector. The total charge collected by the rear face of the detector was measured and compared with the total charge collected by the front face (strips). Secondly, it was shown that by utilising leading-edge discriminator time walk, it was possible to determine the position of a detection along a strip. Using this information in conjunction with the position determined from the charge division permits a reduction of background contributions. Background reduction using timing is typically implemented using constant fraction discriminators (CFDs), which give more accurate time measurements. However, we demonstrate that due to the mode of operation of RSDs, leading edge discriminators can be used instead. Therefore, the presented methods may be useful in reducing the cost of electronic components in silicon detector arrays.

The following section provides a detailed description of each background reduction method

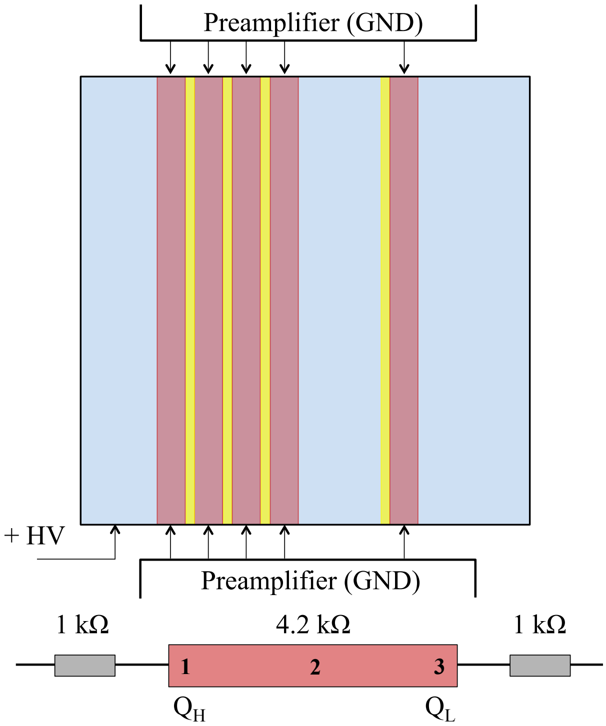

Figure 2: (color online) Schematic diagram of a *Hamamatsu* resistive charge-division strip detector. The upper image shows the face of the detector and the lower image illustrates the charge division mechanism along a single strip. The large rear contact covers the whole detector area and is used to apply the reverse bias. The front strips are held at ground and energy signals are taken from each end. The charges collected at the *high* and *low* ends of the strip are labelled Q_H and Q_L. The hit positions labelled as 1, 2 and 3 are discussed in the text.

and their implementation in the experimental hardware. Section 3 then presents the results of these techniques when applied to measuring radiation from a triple-α source and when measuring the ^{12}C(^{4}He,α)$\alpha\alpha\alpha$ breakup reaction.

2. Experimental method

Under investigation in this study is the *Hamamatsu* 16-strip RSD [Hamamatsu Photonics Ltd] [12]. This has an active area of 5 × 5 cm^2 and a thickness of 500 μm. Although the Hamamatsu detector is no longer in commercial production, the Micron *X1* detector [Micron Semiconductor Ltd] operates in the same way and is currently implemented in the TIARA array, which has recently been commissioned for use at the Texas A&M Cyclotron Institute [11, 13]. The research outcomes from this paper can, in principle, be applied to any detector which utilises resistive charge division in one dimension.

The two background reduction methods were implemented into the front-end electronics as shown in Fig. 3. The complete set-up utilised a total of five Mesytec MPR preamplifiers, seven CAEN N568B spectroscopy amplifiers, five CAEN V895 leading edge discriminators, one CAEN V775 time-to-digital converter (TDC) and four Silena VME 9418 ADCs. Figure 3 shows the integration of the Hamamatsu RSD into the experimental set-up, which was sufficient to

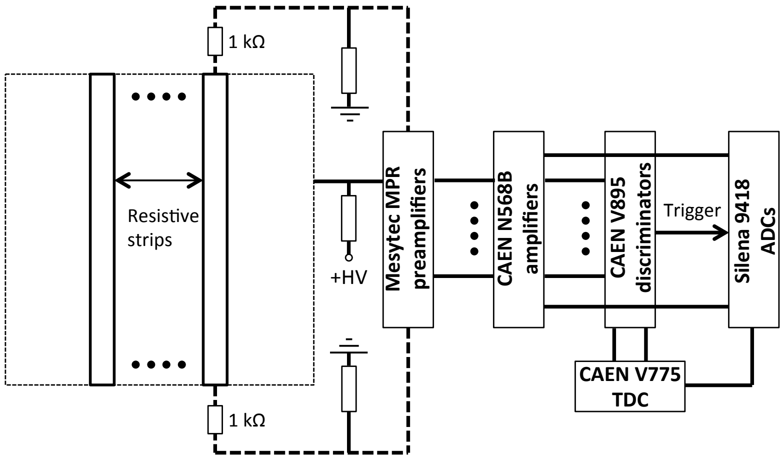

Figure 3: Block diagram of the front-end electronics. The dots signify multiple channels. The triggering logic and the inputs to the TDC are discussed in the text.

measure radiation from an α source. In order to measure the ^{12}C(^{4}He,α)$\alpha\alpha\alpha$ breakup reaction at 40 MeV bombarding energy, an extra DSSD telescope (64 channels) was introduced. When measuring this reaction, the ADC trigger required that three or more detector channels fired in coincidence, across the whole detector array. This condition was implemented across the daisy-chained V895 discriminators and required no external logic circuit. When measuring radiation from the triple-α source, a singles trigger was implemented. Micron *W1* detectors of 500 and 65 μm thickness were used in the DSSD telescope together with a single RSD detector. Respectively, the telescope and RSD were placed at distances of 9.8 and 8.3 cm from a ^{12}C target and at centre angles of −90° and +30° with respect to the beam axis.

The layout of the detectors inside the vacuum chamber to measure this reaction is shown in Fig. 4. The α particle from the beam is scattered into the DSSD telescope. The placement of the detectors maximises the probability that all three α particles resulting from the breakup of the recoiling ^{12}C (if it is in the near-threshold Hoyle state at 7.65 MeV) hit the single RSD. This provides complete reaction kinematics. The target was fixed normal to the target plane at 40° to the beam axis. This reduced the energy losses of the α particles before they hit the RSD. Experimental measurements were performed at the University of Birmingham MC40 cyclotron facility. The ^{4}He beam was in a Q = 2$^+$ charge state and data were acquired at a beam current of 3 enA for three hours. Radiation from the triple-α calibration source was measured for two hours.

The first technique was simple to apply in the hardware; the rear contact of the detector was biased via a preamplifier, rather than directly from the power supply, in order for the charge collected by this contact to be analysed. From here, this signal, along with those from the strips, was amplified, discriminated and passed to the ADC before being read-out for analysis in software. Due to the detection mechanism described in section 1, on average, the same number of electrons must be collected by the rear contact as the number of holes collected by the front strips. This condition applies regardless of the hit multiplicity. Provided each detector is correctly calibrated in energy (using a mixed ^{239}Pu, ^{241}Am and ^{244}Cm source), demanding that the same energy is collected by the rear contact as the sum of the energies on the front strips, provides a way to veto events which include triggers from noise. The results of applying this method are given in

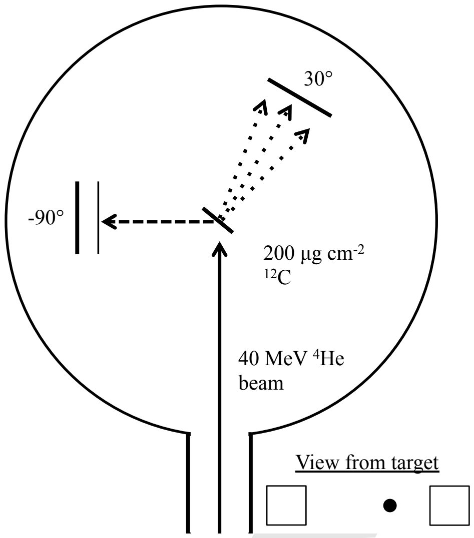

Figure 4: Chamber diagram marking the detector angles with respect to the beam direction. The solid line marks the beam direction, the dashed line marks the path of the scattered beam, and the dotted lines represent the α particles emitted during the breakup of ^{12}C.

section 3.1.

In order to apply the second background reduction method, both the high and low signals from every resistive detector strip were amplified and passed to leading edge discriminators. Each discriminator channel was set to a similar level of around 2.5 MeV. The differential ECL outputs from the discriminators were then inputted to the TDC as start signals. When measuring the ^{12}C(^{4}He,α)$\alpha\alpha\alpha$ breakup reaction, a delayed *or* signal from the rear detector of the separate DSSD telescope was chosen as the common stop, since it provides an external reference time. Setting all TDC channels to have a common stop signal meant that the absolute time difference between the high and low signals, for a given strip, could be calculated. This method was not applied when measuring α radiation from a source, since each particle only strikes the RSD and no external reference signal was available for a stop.

In previous work, the timing characteristics of two-dimensional resistive detectors were analysed and a relationship between the hit position and the timing output was identified [14]. This was qualitatively attributed to a large charge collection time on the resistive detector layer. In the present study, the TDC was used to measure the time walk arising from the leading edge discriminators and determine the hit position of a particle along a strip. Time walk corresponds to the situation shown in Fig. 5, where two pulses with identical shape and time of occurrence, but different amplitudes, will cross a constant discriminator threshold at different times [15]. If a particle hits a resistive strip, the pulses recorded at each end of the strip arrive at approximately the same time. Once integrated by the preamplifier, the pulses possess different amplitudes due to the resistance of the strip. These pulses are amplified and examined by leading edge discriminators. Since the resulting time walk depends on the amplitude of each pulse, it can be related to the charge division and, hence, to the position of a hit along a detector strip. Due to the nearly Gaussian pulse shapes (using a 1 μs shaping time), the relationship between time walk and hit position is slightly non-linear and depends on the pulse heights relative to the threshold.

Figure 5: Illustration of the time-walk effect, Δt, of leading edge discrimination.

Alone, this method tells us no more about the position of a hit than when using the standard charge division. However, when the two methods are used simultaneously, it is possible to check for consistency between the positions calculated by each. For example, given a particular hit position and, therefore, a particular charge division, there is a defined discriminator time walk which must also be measured (see Fig. 5). If the discriminator triggers on the noise, or the high and low signals correspond to particles associated with different events (random coincidences), the time difference between the high and low signals will be uncorrelated. Removing events where the time difference between the pulses is uncorrelated with the charge division was found to improve the overall signal-to-background ratio (SBR) without a notable drop in efficiency. A typical experiment utilising timing information will use CFDs and demand that all measured pulses lie within a narrow time window. This ensures that all signals in an event correspond to the same nuclear reaction (minimising random coincidences) and do not include uncorrelated triggers on the baseline noise. This paper demonstrates that, due to the RSD mechanism, CFDs are not necessary for timing measurements when using these detectors.

3. Analysis and results

Background reduction was quantified in two ways. When measuring radiation from the α source, it was simple to examine any background contributions to the energy spectrum. Since the spectrum of discrete energies is known, any noise will manifest as a background to the three features, which arise from the α-decay of the source isotopes. The same cannot be said when measuring the breakup of ^{12}C since, for any given event, the measured α particles may possess a range of energies.

Instead, the *sum energy* of each event was used to gauge the background contributions. Due to energy conservation, the sum of the energies of the four final state particles from the ^{12}C(^{4}He,α)$\alpha\alpha\alpha$ reaction minus the breakup Q value (−7.27 MeV) must equal the 40 MeV beam energy, within the experimental resolution. Events which do not meet this condition are identified as background, likely arising from triggers on noise or due to random coincidences with

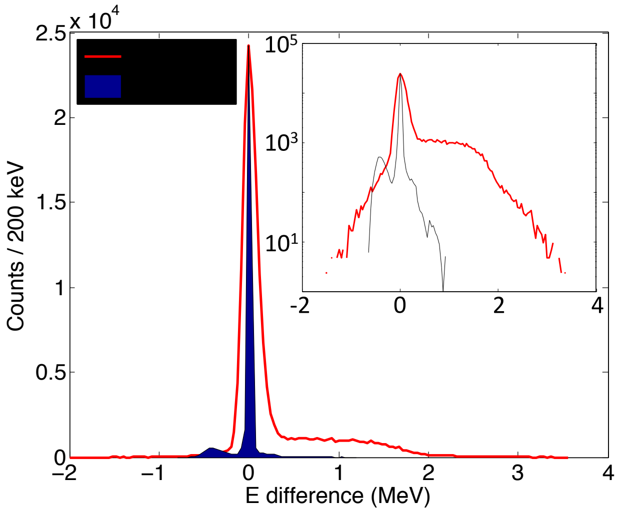

Figure 6: (color online) Difference in energy between the front strips and the rear detector contact. The inset shows the same data on a logarithmic scale. The filled histogram shows the multiplicity-1 α source measurements. The thick (red) line depicts the multiplicity-3 data acquired when measuring the ^{12}C breakup reaction. Most events are centred around an energy difference of zero (within the experimental energy resolution). See text for details.

particles associated with separate events. Particles striking particularly close to the inter-strip region will cause some charge sharing between the strips, and these events may also manifest as a background to the sum energy peak. The area of the sum energy peak when compared with the background was used to calculate the SBR. In the data analysis, only complete kinematics events are considered; a single α particle hit in the DSSD telescope was demanded in coincidence with three strips on the RSD.

This particular breakup reaction and detector arrangement was chosen because of its unambiguous kinematic signature. Contaminant reactions ^{12}C(^{4}He,^{8}Be)^{8}Be and ^{12}C(^{4}He,^{16}O*) have the same 4α final state but most often result in a different particle distribution across the detector array to that shown in Fig. 4. These reactions have the same -7.27 MeV breakup Q value and so are distinguishable from noise in the sum energy spectrum. The large 90° angle of the telescope detectors minimises the contributions of direct beam scattering into the telescope causing false coincidences.

3.1. *Front and rear contact energy matching*

Figure 6 shows the difference between the total energy collected by the front strips minus the energy collected by the rear contact, plotted as a histogram for all events. The shaded histogram depicts the data acquired when measuring the α source (43973 events). The thick red line shows the ^{12}C(^{4}He,α)$\alpha\alpha\alpha$ reaction data (70656 events). The peaks have been scaled to have the same amplitude for a visual comparison. The peaks centred on zero in Fig. 6 demonstrate that for the majority of events, the energies collected by the front strips equals that of the rear contact. The width of the peaks is due to the detector energy resolution (FWHM ≈120 keV for the RSD).

For both data sets, substantial data reside outside of this main peak and are identified as contributions from sources of background. A software gate was applied in order to select the data which reside inside these peaks. Data within 3σ of the peak centroid were taken for further

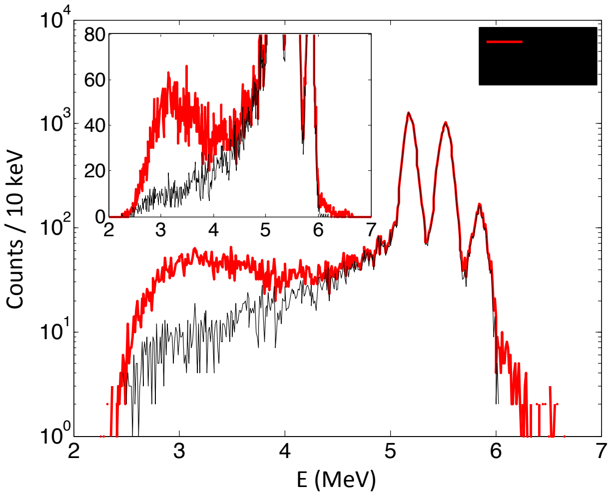

Figure 7: (color online) The measured α-source spectrum before (thick red line) and after (thin black line) the energy matching condition was applied. The main plot has a logarithmic y-axis and the inset shows the same data plotted with a linear y scaling.

analysis. Figure 7 shows the measured spectrum of α particle energies before and after this software gate was applied. The thin, black histogram (after the gate was applied) shows a much smaller contribution at lower energies, when compared with the thick, red histogram (before the gate was applied). These events could be due to triggers on the noise, or due to incomplete charge collection, when a particle strikes the inter-strip region. A total of 12% of events were rejected.

Figure 8 shows the sum energy peak for full kinematics breakup events before and after the software gate was applied to the plot shown in figure 6. The width of these peaks is due to the detector energy resolution ($\approx$60 keV for the DSSDs and $\approx$120 keV for the RSD when measuring a triple-α source), the energy losses of the particles and the beam in the 200 μg/cm^2 target, and the beam energy spread. This was verified by Monte-Carlo simulations of the reaction and detector geometry. The Monte-Carlo code is discussed in Refs. [16, 17]. The background beneath the sum energy peak is reduced after the gate is applied. In both cases, it can be seen that the background contributions are reduced by around one order of magnitude in some places. Based on the ratio of the area of the sum energy peak to that of the background area (phenomenologically modelled as a quartic polynomial to reproduce the correct shape) an improvement of the SBR from 8.8(2) to 35.2(16) was found. This corresponds to an improvement by a factor of 4.0(2).

3.2. *Time walk*

None of the TDC channels were calibrated, however, it was ensured that consistent wire lengths and delays were used throughout the electronics chain in order for pulses corresponding to a single reaction to enter the TDC at approximately the same time. The maximum TDC time range of 1.2 μs was used. The the charge propagation time from one end of the strip to the other is about 50 ns, thus, this has a negligible effect here. Each TDC output was recorded to disk. Figure 9 shows the difference in time between signals recorded at each end of a strip (in arbitrary TDC units) plotted against the calculated position of a detector hit based on the charge division. As expected, the time difference due to time walk varies approximately linearly with

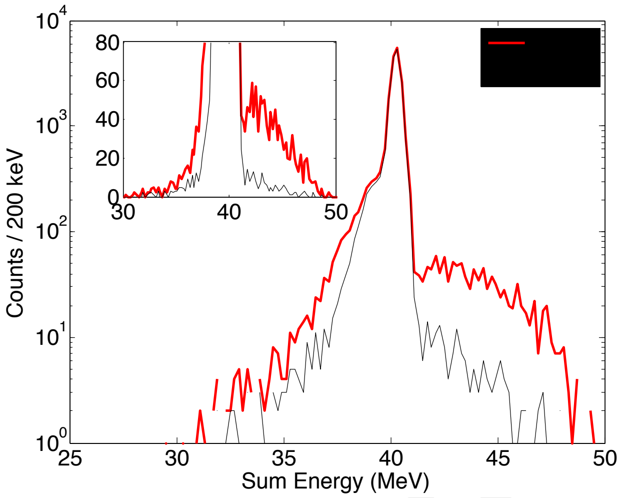

Figure 8: (color online) The measured sum energy spectrum before (thick red line) and after (thin black line) the energy matching condition was applied. The main plot has a logarithmic y-axis scale and the inset has a linear y-axis scale.

the detector hit position. Towards the end of each strip, some non-linearity is observed since this corresponds to a situation where one of the pulses heights is much nearer to the discriminator threshold and, thus, the time difference is more sensitive to the Gaussian pulse shape. This behaviour is reproduced when calculations of leading edge triggering on Gaussian pulse shapes were performed. Along with the data points which lie along the expected diagonal bands, each plot shows a roughly uniform background of points with no clear correlation between the time walk and charge division. These points are identified as background contributions.

Plots corresponding to different cuts in strip energy are shown in Fig. 9. The TDC time difference is more sensitive to the position (charge division) for low energy pulses, which manifests as a steeper gradient. With reference to Fig. 5, due to the Gaussian pulse shape, a small change in the amplitude of the lower peak will result in a relatively large change in the time walk. This is because this signals peak closer to the discriminator thresholds. On the other hand, for higher energy detections, the discriminator threshold is low compared to both the high and low signals, and a weaker dependence of the time walk on the hit position is observed. This effect manifests as a shallowing of the gradients of the plots shown in Fig. 9 as the energy is increased.

The plots of Fig. 9 were constructed for a number of different energy cuts on the experimental data, and on a strip-by-strip basis. Assuming a linear relationship between time difference and position, a linear function was fit to the scatter plots using the `polyfit` least squares fitting algorithm [`Matlab 2012a`]. The gradient of the resulting fit, for a single detector strip, as a function of energy is given by the points with error bars in Fig. 10. The blue line shows the expected behaviour from calculations of the leading edge discrimination process on Gaussian pulses. Since the time units given by the TDC are not calibrated, a linear scaling in the vertical direction was applied in order for the predicted behaviour to best fit the experimental data.

Only experimental data points that lay within the diagonal bands shown in Fig. 9 were selected in the analysis software. In order to achieve this, it was required that the gradient of each band (assumed to be linear) was known as a function of energy, for each detector strip. To

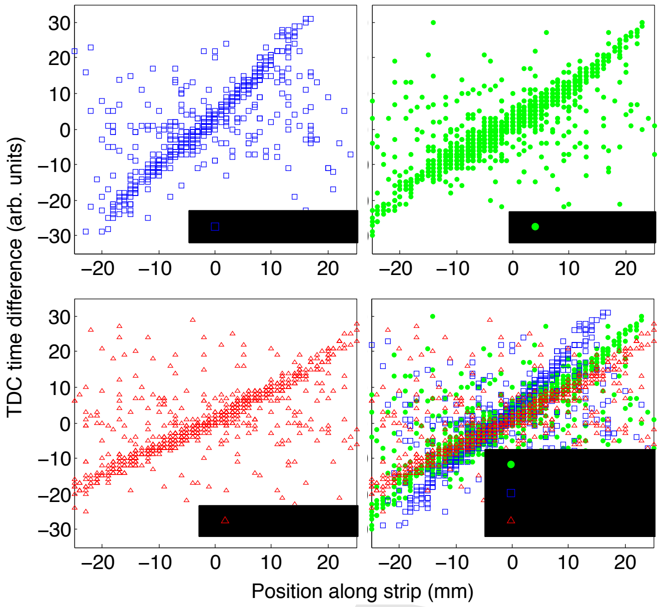

Figure 9: (color online) Position of a hit calculated from the resistive charge division vs the trigger time difference between the pulses at each end of the strip. The data show some non-linearity towards the ends of the strips since this corresponds to the situation where one of the pulse heights is near to the discriminator level. See text for details.

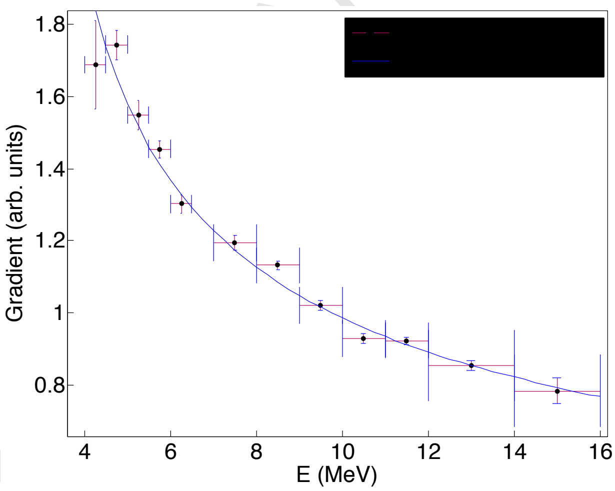

Figure 10: (color online) Gradient of the position vs TDC time difference plots, for different detected energies. The points with error bars show the experimental data. More data exist at lower energies and so these points have smaller energy bin widths. The (blue) line shows the predictions of time walk. Since the time difference is in arbitrary units, the line has been scaled vertically to best fit the experimental data.

simplify this process, as an approximation, the data shown in Fig. 10 were phenomenologically modelled as an exponential of the form

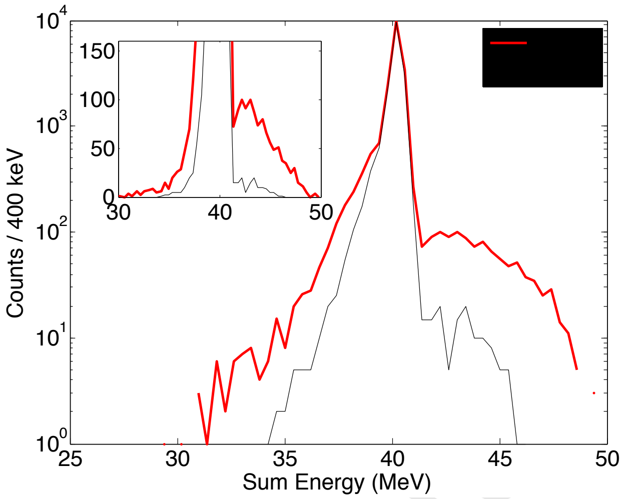

Figure 11: (color online) The measured sum energy spectrum before (thick red line) and after (thin black line) the time walk condition was applied. The main plot has a logarithmic y-axis scale and the inset has a linear y-axis scale.

$$m = \alpha + \beta e^{-\gamma E}, \tag{2}$$

where m is the gradient of the band at a particular energy E, and α, β and γ are fit parameters to be determined. With this relationship known for each detector strip, it was possible to predict, for a given calculated hit position, what the expected time walk should be. Data that lie within the typical width of each band (FWHM found to be $\approx$7 TDC units) were selected for further analysis. Data outside this region were assumed to be events that include triggers by noise. Figure 11 shows the sum energy spectrum before and after this TDC cut was applied in the analysis software. Based on the ratio of the area of the sum energy peak to that of the background area (modelled as a quartic polynomial) an improvement of the SBR from 8.8(2) to 29.2(28) was found. This leads to an improvement by a factor of 3.7(4). When both background reduction methods were applied together, a SBR of 50.0(24) was measured, giving a total improvement factor of 5.7(3).

4. Conclusions

Two background reduction methods have been developed for resistive charge-division strip detectors. Despite both providing a similar improvement in the recorded SBR, the authors advocate the first method of front and rear contact energy matching for practical use at the current time. It was simple to apply in the experimental hardware and required very little analysis in post-processing. In contrast, a 32-channel TDC is required in order to apply the second method, along with substantial analysis in software. Nonetheless, this timing method was proven to be an effective way of suppressing background contributions, and demonstrates that more costly CFDs are not required for timing when using RSDs.

The authors encourage further investigation into these two methods in the future. Their relative effectiveness should be evaluated for energies lower than 2.5 MeV. This was prohibited by the set-up employed in this experiment due to the reaction kinematics of the ^{12}C breakup. Although both methods show a similar improvement in the SBR for the current measurements, it is possible that this changes as the energies and thresholds are lowered. Further, the presented methods could be applied to the more modern Micron *X1* detector since this is currently used in research.

5. Acknowledgements

The authors gratefully acknowledge all of the staff at the Birmingham MC40 cyclotron for providing the ^{4}He beam. This work was funded by the United Kingdom Science and Technology Facilities Council (STFC) under grant number ST/L005751/1.

6. References

[1] E. H. M. Heijne, Nucl. Instrum. Methods. A 591 (2008) 6-13.
[2] A. Longoni, G. Lutz, A. Schwarz, L. Struder, T. Davinson, A.C. Shotter, E.W. Macdonald, S.V. Springham, P. Jobanputra, A.J. Stephens, S.L. Thomas, Nucl. Instrum. Methods. A 288.1, (1990) 245-249.
[3] G. Lutz, Nucl. Instrum. Methods. A 367.1 (1995) 21-33.
[4] H. O. U. Fynbo and C. Aa. Diget, Hyperfine Interactions 223:1 (2014) 103.
[5] M. Freer et al., Phys. Rev. C 49, R1751 (1994).
[6] M. Itoh et al., Phys. Rev. Lett. 113, 102501 (2014).
[7] R. Smith et al., Phys. Rev. Lett. 119, 132502 (2017).
[8] P. J. Leask, Ph.D. thesis, University of Birmingham (2000).
[9] W. N. Catford and R. C. Lemmon and C. N. Timis and M. Labiche and L. Caballero and R. Chapman, AIP Conference Proceedings, 704 (2004) 185-194.
[10] A. Robinson, University of Surrey internal report, (2006).
[11] M. Labiche, et al. Nucl. Instrum. Methods. A 614.3 (2010) 439-448.
[12] Hamamatsu Photonics UK LTD, Welwyn Garden City, Hertfordshire <http://www.hamamatsu.com>.
[13] Micron Semiconductor LTD, Lancing, Sussex, UK <http://www.micronsemiconductor.co.uk>.
[14] C.E. Wu, Y.L. Ye, D.X. Jiang, T. Zheng, H. Hua, Z.H. Li, X.Q. Li, Y.C. Ge, G.L. Zhang, D.Y. Pang, J. Wang, J.L. Lou, Nucl. Instrum. Methods. A 555 1-2 (2005) 266-269.
[15] G. F. Knoll, Radiation detection and measurement. John Wiley & Sons, (2010) 660.
[16] N. Curtis, N. M. Clarke, B. R. Fulton, S. J. Hall, M. J. Leddy, A. S. J. Murphy, J. S. Pople, R. P. Ward, W. N. Catford, G. J. Gyapong, S. M. Singer, S. P. G. Chappell, S. P. Fox, C. D. Jones, D. L. Watson, W. D. M. Rae, and P. M. Simmons, Phys. Rev. C 51, 1554 (1995).
[17] N. Curtis, A. S. J. Murphy, N. M. Clarke, M. Freer, B. R. Fulton, S. J. Hall, M. J. Leddy, J. S. Pople, G. Tungate, R. P. Ward, W. N. Catford, G. J. Gyapong, S. M. Singer, S. P. G. Chappell, S. P. Fox, C. D. Jones, D. L. Watson, W. D. M. Rae, P. M. Simmons, and P. H. Regan, Phys. Rev. C 53, 1804 (1996).